# Journal of Intelligent Material Systems and Structures

---

**Extending Point-sensor Performance by Incorporating Distributed-sensors and Window Functions**

Yu-Hsiang Hsu and Chih-Kung Lee

The online version of this article can be found at:

---

Additional services and information for *Journal of Intelligent Material Systems and Structures* can be found at:

**Email Alerts:** http://jim.sagepub.com/cgi/alerts

**Subscriptions:** http://jim.sagepub.com/subscriptions

**Reprints:** http://www.sagepub.com/journalsReprints.nav

**Permissions:** http://www.sagepub.co.uk/journalsPermissions.nav

**Citations** http://jim.sagepub.com/cgi/content/refs/16/2/149

# Extending Point-sensor Performance by Incorporating Distributed-sensors and Window Functions

Yu-Hsiang Hsu and Chih-Kung Lee*

*Institute of Applied Mechanics, National Taiwan University, Taipei, Taiwan 106, China*

**ABSTRACT:** By integrating the methodologies of window functions and the method of image, the performance of the traditional piezoelectric point and distributed sensors, such as accelerometers, can be tailored by modifying their transfer functions in the spatial domain. The approach used in extending the sensor performance consists of developing a series of methodologies that can tailor the gain of the sensor transfer function while keeping the phase of the sensor transfer function intact. We can show that these spatially introduced design methodologies bypass the Bode gain–phase theorem, which states that gain and phase are interrelated for all minimum phase systems. The effects of adopting these sensors to flexible structure control and point sensors are examined in detail. It can also be shown that a series of low-pass filters, which exerts autonomous behavior between the gain and the phase of the sensor transfer function, can be introduced to significantly influence the performance of the sensing or controlling loops that incorporates these sensors. In addition, variables such as the power of the window functions adopted, the desired corner frequency, the length of the sensor structure, etc., all can be shown to have a decisive impact on the performance of the newly invented sensors. Both theoretical and experimental results of the underlying principles, design methodologies, and implementation process of these newly invented sensors are detailed.

*Key Words:* point sensor, distributed sensor, piezoelectricity, window function, accelerometer

## INTRODUCTION

**P**IEZOELECTRIC materials have been widely used in many fields including the design and fabrication of sensors and actuators. The influence of placement and the interactions of distributed piezoelectric sensors and actuators have been studied by many researchers (Prak et al., 1992; Tzou et al., 1993; Tzou and Hollkamp, 1994; Preumont and Francois, 1999). Over the years, it has been well understood that distributed sensors and actuators exert their influence on structures by mapping an appropriate strain distribution. The application of a spatial–filter concept to flexible structure control was first examined by Collins and Miller (Miller et al., 1990) and it gave us the first indication that autonomous gain–phase tailoring was possible. The striking characteristic of this new class of piezoelectric distributed sensors was that it appeared to bypass the limitations imposed by the Bode gain–phase theorem (Bode, 1945) that states that the gain and phase of causal sensors cannot be changed independently. Even after more than 20 years of extensive research and development, distributed sensors such as spatial sensors (Miller et al., 1990) or modal

sensors (Lee, 1992) still do not have the same popularity as that of piezoelectric point sensors. The main reason lies in the fact that piezoelectric distributed sensors must be redesigned for every structure since they are specific with respect to the structure of interest. On the other hand, point sensors also suffer two major limitations, which are (1) they cannot integrate structure information known a priori, and (2) the available bandwidth of the point piezoelectric sensor is closely correlated to the mechanical structure of the sensor itself.

In this article, we present a whole new class of piezoelectric sensors developed over the last eight years, which can tailor the system gain and phase independently. To signify that these newly invented sensors have an autonomous gain–phase relationship, they have been called APROPOS devices, an acronym for Autonomous Phase–gain ROtation/Linear Piezoelectric Optimal Sensing, of which the basic design concepts of this device was first proposed by the authors in 2002 (Hsu and Lee, 2002, 2003). The design view of an APROPOS device is to rewrite the sensor equation of a distributed sensor into two-sided Laplace transforms such that no-phase-delay filters are thus able to be implemented in a spatial domain. In a earlier study, no-phase-delay low-pass filters were implemented successfully by using the method of image and the superposition nature of

---
*Author to whom correspondence should be addressed.
E-mail: cklee@ntu.edu.tw

integration (Hsu and Lee, 2002, 2003). In that study, the filters were implemented by subtracting a sine or a cosine function to eliminate the nonzero weighting of the base function to become zero at the boundaries. It was seen that the no-phase-delay filters were determined only by the chosen base of the weighting function, which was a simple and straightforward method.

In this article, we introduce window functions into the sensor design process. By using them various design parameters such as the power of the window functions adopted, the desired corner frequency, and the length of the sensor structure can be embedded into the sensor transfer function. With this newly introduced design concept, the characteristics and performance of the induced no-phase-delay low-pass filter can be further tailored without changing the chosen base of the weighting function. By incorporating the proposed design methodology into the design of Point-distributed sensors (PoD) which was first proposed by the authors in earlier works (Hsu and Lee, 2002, 2003), a series of new point sensors can be implemented. Both the theoretical and the experimental results of adopting the APROPOS device to applications such as the PoD sensors and the flexible structure control will be detailed herein.

## THEORY OF PIEZOELECTRIC LAMINATES

The basic theory relating to piezoelectric laminates (Lee and Moon, 1990; Lee, 1992) is briefly reviewed first. Piezoelectricity, first discovered by Pierre and Jacques Curie (Cady, 1946), basically indicates that if stress is applied to a piezoelectric material, charges can be sensed from the surface. In addition, mechanical deformation results whenever an external electric field is applied to the piezoelectric materials. Polyvinylidene fluoride ($PVF_2$), a polymeric piezoelectric material first discovered in 1969 by Kawai, was used throughout the course of this research. As $PVF_2$ possesses mm2 symmetry (Kawai, 1969; Lee, 1992), only five piezoelectric stress constants $d_{31}$, $d_{32}$, $d_{33}$, $d_{24}$, and $d_{15}$ are needed to completely describe its piezoelectric effect.

Four sets of constants are typically used to model piezoelectric materials (Cady, 1946; Lee, 1990, 1992), i.e., the piezoelectric charge constants $d$, and $e$, and the piezoelectric voltage constants $g$ and $h$. Materials with a high piezoelectric charge constant $d$ are typically chosen when designing actuators. On the other hand, materials with a high piezoelectric voltage constant $g$ are typically chosen when designing sensors. When written in an IEEE compact matrix notation, the constitutive equations of piezoelectric materials can be written as follows: (Lee, 1990; ANSI/IEEE Standard 176, 1987)

$$S_p = s_{pq}^E T_q + d_{ip}E_i, \quad D_i = d_{ip}T_q + \varepsilon_{ij}^T E_k, \quad \text{(1a,b)}$$

where $i$, $k = 1$–3, $p$, $q = 1$–6, $T_p$, $S_q$ are stress and strain; and $D_i$ and $E_k$ represent the electric displacement and the electric field, $s_{pq}^E$ is the elastic compliance constant, $\varepsilon_{ij}^T$ is the permittivity constant, and the superscripts 'E' and 'T' indicate the E and T fields, which are constants. As piezoelectric materials in thin sheet form mounted on thin layer sensing structures is the main configuration examined in this article, a plane stress approximation was adopted. That is, Equation (1b) can be simplified to be

$$D_3 = \varepsilon_{33}E_3 + d_{31}P_1(x,y)T_1 + d_{32}P_2(x,y)T_2$$
$$+ d_{36}P_6(x,y)T_6, \quad \text{(2)}$$

where $P(x,y)$ represents the relative polarization strength of the piezoelectric lamina and has a value $\leq 1$. The polarization strength was set as 1 throughout the piezoelectric thin film in this article. In other words, the piezoelectric thin film was uniformly polarized.

Due to the thin sheet form of the $PVF_2$ adopted, the charge induced can only be detected from the thickness direction. Adopting the Gauss' Law to find the closed circuit charge signals detectable by surface electrodes, the charge signals generated by the $k$th lamina of a three-layered $PVF_2$–shim metal–$PVF_2$ laminate (Figure 1) becomes (Lee, 1987, 1992; Lee and Moon, 1990)

$$q_k(t) = -z_k^0 \int_{\overline{S}} F(x,y)\left[e_{31}\frac{\partial^2 w}{\partial x^2} + e_{32}\frac{\partial^2 w}{\partial y^2} + 2e_{36}\frac{\partial^2 w}{\partial x \partial y}\right]dx\,dy,$$

$$\text{(3)}$$

where $k = 1$, 3; $F(x,y)$ represents the effective surface electrode, i.e., $F(x,y) = 1$ if the piezoelectric lamina is covered by the surface electrode on both the top and the bottom sides and $F(x,y) = 0$ if either the top or the bottom surface electrode of the piezoelectric lamina is missing. It should be noted that Equation (3) was obtained by using the plane-stress approximation as the piezoelectric lamina being considered was assumed to be in thin sheet form since this type of deformation
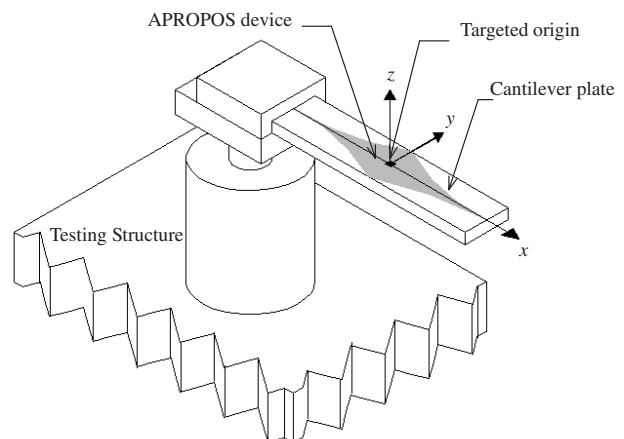


**Figure 1.** Schematic of a PoD sensor using a one-dimensional cantilever plate as the base sensor structure.

$w(x, y, t)$ is most suitable to modeling a two-dimensional thin plate.

Consider the one-dimensional case of Equation (3) where a one-dimensional plate which assumes $w = w(x, t)$ is considered as the sensor structure (Figure 1). It should be noted that a one-dimensional plate is similar to a beam with some notable differences. The main difference lies in the fact that a plane-stress approximation can be adapted to the thickness direction of the thin plate while a plane-strain approximation can be adapted along the width direction. On the other hand, the plane-strain approximation can be adapted to the thickness direction of a beam while a plane-stress approximation can be adapted to the width direction of the beam. This understanding basically means that the equations representing a one-dimensional plate and the beam can replace each other by modifying the stiffness term of the equations, which are identical to that of the plane-stress and the plane-strain conversion typically found in standard elasticity textbooks (Fung, 1965). The principal axes of the piezoelectric thin sheets were chosen to coincide with the principal axes of the one-dimensional plate, and with the above-mentioned approximations. Thus, Equation (3) can be reduced to

$$q_k(t) = -z_k^0 e_{31} \int_{a_1}^{a_2} R(x) \frac{\partial^2 w}{\partial x^2} dx \qquad (4)$$

where

$$R(x) = \int_{-b/2}^{b/2} F(x, y) \, dy \qquad (5)$$

is the effective surface electrode for a one-dimensional case, the integrating region $a_1$–$a_2$ represents the boundaries of the piezoelectric thin lamina, and $b$ represents the width of the PVF$_2$ lamina. We know that Equation (4) forms the basis of most distributed piezoelectric sensors (Miller et al., 1990; Lee, 1992; Hsu and Lee, 2002). The new APROPOS device-based sensors discussed in this article are also based on Equation (4) as well. More specifically, all of the autonomous gain–phase sensors can be introduced into the frequency response of a sensing structure by choosing a proper effective surface electrode $R(x)$ with the understanding presented herein.

Taking a one-dimensional cantilever plate (Figure 1) with a pure bending assumption formed by laminating two layers of piezoelectric laminate of thickness $h_p$ on each side of a stainless steel shim of thickness $h_s$ as the sensing structure, and neglecting its damping effect, the governing equation of displacement $w$ can be shown to be (Lee, 1990, 1992; Lee and Moon, 1990; Tzou et al., 1994):

$$D_{11} \frac{\partial^4 w(x,t)}{\partial x^4} + \rho A \frac{\partial^2 w(x,t)}{\partial t^2} = 0 \qquad (6)$$

where $\rho A = (\rho_s h_s + 2\rho_p h_p)b$ is the product of density $\rho$ and the cross section of the plate $A$, and where subscripts $p$ and $s$ represent the piezoelectric and the stainless steel shim. The flexural rigidity $D_{11}$ is $[h_s^3 E_s/(12(1-\nu_s^2)) + h_p(h_s^2/2 + h_s h_p + 2h_p^2/3)(E_p/(1-\nu_p^2))]b$, where $\nu_s$ is the Poisson's ratio of the stainless shim, respectively (Lee, 1992). It should be noted that $D_{11}$ is different from the bending stiffness of a beam even if the mechanical stiffness of the piezoelectric lamina is neglected. More specifically, as the mechanical stiffness of a piezoelectric thin lamina is much smaller than that of a stainless steel shim plate, smaller by about 67 times, its mechanical stiffness can be neglected by setting $E_p = 0$ herein. In this case, $D_{11}$ becomes $[h_s^3 E_s/(12(1-\nu_s^2))]b$, which is $E_s I/(1-\nu_s^2)$ with $I = bh_s^3/12$ as the moment of inertia of an equal width beam. The difference of $1/(1-\nu_s^2)$ can be traced back to the conversion of the plane-stress and plane-strain approximation in elasticity (Fung, 1965). Considering that the Poisson's ratio of a stainless shim is approximately 0.3, the influence of $1/(1-\nu_s^2)$ is about 10% and therefore cannot be neglected.

Considering the harmonic excitation case $w(x, t) = w(x)e^{j\omega t}$, Equation (6) can be rewritten as

$$\frac{\partial^4 w}{\partial x^4} - k^4 w(x) = 0, \qquad (7)$$

where

$$k^4 = \frac{\rho A}{D_{11}} \omega^2 \qquad (8a)$$

is the dispersion relationship, $k$ is the wave number, and $\omega$ is the angular frequency. The dispersion relationship in Equation (8a) can be separated into two equations, which are shown to be

$$k^2 = \sqrt{\frac{\rho A}{D_{11}}} \omega, \qquad (8b)$$

$$-k^2 = \sqrt{\frac{\rho A}{D_{11}}} \omega, \qquad (8c)$$

where Equation (8b) represents the characteristics of one-dimensional plate $jk$ and $-jk$, and Equation (8c) represents the other two characteristics of the one-dimensional plate $k$ and $-k$. The general solution $w(x, t)$ for Equations (6)–(8) can be expressed as:

$$w(x, t) = \left[ w_{lp}e^{jkx} + w_{le}e^{kx} + w_{rp}e^{-jkx} + w_{re}e^{-kx} \right]e^{j\omega t}, \quad (9)$$

where $w_{lp}$ and $w_{rp}$ are the wave mode amplitude of the left and the right propagating wave modes, $w_{le}$ and $w_{re}$ are the wave mode amplitude of the evanescent wave modes, and $j = (-1)^{1/2}$. These four constants are the functions of the wave number $k$ only, and will have different magnitudes for different boundary conditions. These four wave modes and their wave mode amplitudes include full characteristics of the structures and establish

the fundamental concept of the new sensors. That is, wave modes are the main design principle on which the APROPOS devices are based. It can also be shown that by adopting these four wave modes properly, the structure performance characteristics can be tailored at will. Substituting Equation (9) into Equation (4) and assuming that the external vibration is a function of the harmonic wave, the basic sensor equation for the newly invented APROPOS device becomes

$$q(t) = -z_k^0 e_{31} e^{j\omega t} k^2 \int_{a_1}^{a_2} R(x) \Big[ -w_{lp} e^{jkx} + w_{le} e^{kx}$$
$$-w_{rp} e^{-jkx} + w_{re} e^{-kx} \Big] dx$$

$$(10)$$

where $z_k^0$ is the moment arm of the piezoelectric lamina and equals $(h_s + h_p)/2$ for the structure discussed in Figure 1. Equation (10) essentially states that the charge signal generated can be viewed as the superposition of the four wave modes of the structure propagating between the boundaries and the effect of the weighting factors provided by the effective surface electrode, $R(x)$ for each of the wave modes. More specifically, the effective surface electrode, $R(x)$ serves as a weighting function of the wave modes and this understanding forms the fundamental design concept of APROPOS devices. In other words, the transfer function of the sensor structure can be tailored at will by choosing the proper effective surface electrode, $R(x)$.

As already mentioned, the first attempt to use the effective surface electrode, $R(x)$ to implement spatial filters that act like a low-pass filter in gain but does not induce any phase delay was reported in 1990 (Miller et al., 1990). At that time, the influence of boundary conditions and evanescent wave modes $e^{-kx}$ and $e^{kx}$ were ignored, i.e., only the two propagating wave modes $e^{-jkx}$ and $e^{jkx}$ were examined. Earlier, this assumption was justified by mounting a 0.7 m long distributed sensor onto a one-dimensional plate, which was 7.32 m long × 0.1 m wide × 3.175 mm thick. This sensor was also intentionally placed far from the boundaries with the hope that the effect of the boundaries and the evanescent waves could be eliminated. However, this requirement hinders the applicability of the spatial filter to be placed on a point sensor as the distributed sensor size of the spatial filter will be too small to be placed on a sensor structure if it is to be treated as a point sensor. Thus, all effects including those contributed by the evanescent wave modes, the boundary conditions, as well as the propagating wave modes should be considered in order to study the possibility of creating piezoelectric sensors with an autonomous phase–gain relationship for point sensors. The results obtained impact the implementation of flexible structure control.

A two-sided Laplace transform typically used in the electronic signal processing was introduced to serve as the mathematical tool to pursue the autonomous gain–phase filter or the spatial filter concept. That is, each term of Equation (10) can be expressed as follows: (Van Der Pol and Bremmer, 1959; Bracewell, 1978; Grossman, 1988; O'Neil, 1991)

$$L\{R(x); s\} = \int_{-\infty}^{\infty} R(x) e^{-sx} dx \qquad (11)$$

where, $R(x)$ is the equation of the effective surface electrode, and the transform variable $s$ is $jk$, $-jk$, $k$, or $-k$. It should be noted that the characteristic polynomial of the structure is typically expanded on an infinite domain, but the length of the sensor structure is finite and the wave modes propagate in a finite domain. In addition, the amplitude of the wave modes reflected from the boundary is highly dependent on the boundary. To overcome some of the drawbacks mentioned above, the effect of the boundaries on the charge signal generated needs to be taken into consideration. In summary, unlike the strategy (Miller et al., 1990) chosen earlier, which temporarily circumvented the shortcomings of the mathematical model adopted by neglecting the effect of the boundaries and the evanescent wave modes by means of placing a small spatial filter far from the boundary on a very long free-free beam, new mathematical tools were required in order to make Equation (11) as the basis of the foundation of APROPOS devices for general sensor structures. This concept was first proved possible by using the method of image and the superposition characteristic of integration into Equation (10) in 2002 (Hsu and Lee, 2002). This earlier methodology proposed a simple and straightforward design concept to introduce a predetermined no-phase-delay filter into sensor transfer function by choosing a designed base.

In this article, we utilize window functions to introduce additional design parameters into the design of an effective surface electrode. In this newly proposed approach, various characteristics of the induced no-phase-delay filters can be further tailored by using the parameters embedded in the transfer function. We can show that by utilizing the window functions, vastly different boundary conditions can also be taken care of by using the new APROPOS device proposed. Furthermore, with the rapid development of MEMS-based sensors, an APROPOS device provides us with an opportunity to take advantage of the increased freedom extended with the introduction of spatial filters. More specifically, all earlier deficiencies in taking the concept of the spatial filters into the point sensors have their roots in the fact that both the boundary and the evanescent wave effects cannot be neglected in sensors with finite lengths. As the APROPOS device concept takes the four wave modes and the boundary effects into consideration, all the limitations imposed earlier have been eliminated. Considering the transfer function

tailoring capability exerted by the spatially distributed electrode, the APROPOS device have proven to be adaptable as distributed sensors that can be integrated within a point sensor design since they can be implemented on a small sensor structure. This extra freedom makes the concept of a PoD sensor possible, as first proposed by the authors in 2002 (Hsu and Lee, 2002) which is based on the idea of creating a point sensor by incorporating the spatial design freedom of distributed sensors. When this APROPOS device is integrated into a PoD sensor, the point sensor then possesses various sensor characteristics as induced by the window functions. The fundamental concepts of the PoD sensors are briefly described in the following section.

## CONCEPT OF POINT-DISTRIBUTED SENSORS

The available bandwidth of the traditional piezo-electric point sensors is typically limited to only 1/5–1/10 of the first-mode resonant frequency if the sensor is to have less than 10% to 5% gain and phase errors. This is due to the fact that the resonance effect of the first mode will magnify the gain of the sensor for different frequencies, which significantly distorts the signal measured near the resonance. In addition, there will be considerable phase delay when the vibration frequency is measured close to the resonance frequency. Both the errors limit the usable bandwidth of the sensor design. Thus the sensor structures chosen often possess a high first-resonance frequency in order to enlarge their usable bandwidth, which also translates to a low sensitivity at a low-frequency region. This trade-off has been the major design point of all commercial accelerometers. The alternative suggested by this study is to choose a flexible structure to serve as a point sensor (Figure 1), which has a significantly lower first-mode resonant frequency. The APROPOS device concept can then serve as a way to recover the lost bandwidth associated with low-resonant frequency, which is the main thought behind the existence of PoD sensors (Hsu and Lee, 2002). We can show that a no-phase-delay low-pass filter introduced by APROPOS devices offer a design freedom to enhance its bandwidth, not available before.

Figure 2 shows the fundamental concept of using an APROPOS device to design a point sensor, i.e., the PoD sensor, where $G_t(s)$ (dashed dark line) represents the transfer functions of a traditional point sensor, and $G_o(s)$ (thick gray line) represents the transfer function of a flexible structure like the one shown in Figure 1. Note that the transfer function of the point sensor $G_t(s)$ is separated into two segments to represent the traditional point sensors that often adopt a high resonance frequency to obtain an usable-enough bandwidth BW. On the other hand, the flexible sensor structure $G_o(s)$ offers an appropriate low-frequency sensitivity, but only
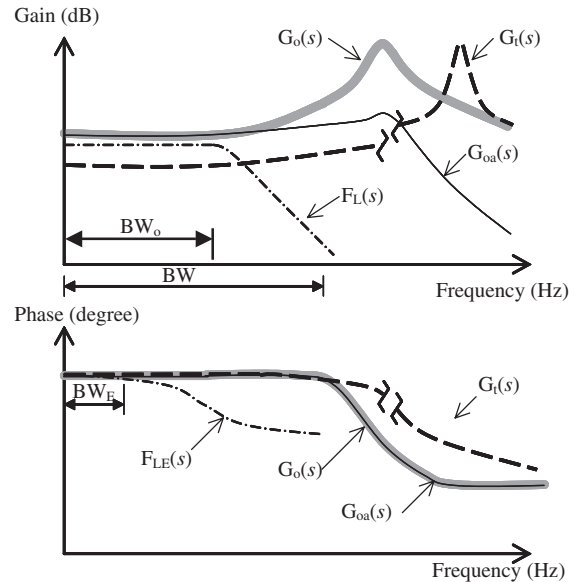


**Figure 2.** Schematic of the effect of an APROPOS device, where $G_t(s)$ (dashed dark line) is the transfer function of a traditional point sensor, $G_o(s)$ (thick gray line) is the transfer function of a flexible structure, $G_{oa}(s)$ is the transfer function of an APROPOS device, $BW_o$ usable bandwidth of $G_o(s)$, $F_L(s)$ is the induced no-phase-delay low-pass filter, BW is the enhanced usable bandwidth, and $BW_E$ is the reduced usable bandwidth by an electrical filter $F_{LE}(s)$.

offers a limited usable bandwidth $BW_o$. The fundamental concept of the PoD sensor is to introduce a kind of no-phase delay low-pass filter $F_L(s)$ like the APROPOS device proposed in this article, into the sensor transfer function $G_o(s)$ to reduce the contribution of structure resonance and push its usable bandwidth from $BW_o$ back to BW, which is shown as $G_{oa}(s)$ (thin dark line). It should be indicated that the usable bandwidth is extended to BW only if the newly introduced low-pass filter does not induce any additional phase delay to the original phase function. This no-phase-delay requirement cannot be met by the traditional electrical filters as phase lag like $F_{LE}(s)$ in Figure 2 with respect to its corner frequency will inevitably reduce the usable one to a much shorter bandwidth $BW_E$.

Therefore, with an APROPOS device, it is possible to increase the usable bandwidth of a sensor without the limitations imposed by the fundamental vibration characteristics of the sensor structure itself. It should be noted again that this autonomous effect is fundamentally different from that of the common electronic filters, which inevitably cause a phase delay for each gain tailoring (Bode, 1945). The concept of the APROPOS device will be detailed further in the following sections.

## CONCEPT OF APROPOS DEVICES

To adopt the two-sided Laplace transform shown in Equation (11) as the mathematical tool for sensor

design, an extra mathematical operation termed "method of image" was further introduced (Graff, 1975). One of the fundamental advantages of utilizing the method of image is that the phase relationship can be taken care of when considering the interaction between the wave modes and the boundaries. The two boundary conditions for the cantilever sensor structure shown in Figure 1 are of a fixed-end and a free-end. Since these two boundary conditions are easy to fabricate and are commonly found, they were examined in detail first. It should be noted that a wave mode can introduce a no-phase delay when it encounters a free-end and will encounter an 180°-phase delay when it is reflected from a fixed-end. More specifically, the wave modes are continuous at the free-end and must be multiplied by a factor of −1 for the fixed-end (Figure 1).

Based on this, the method of image can be adopted to expand the path where wave modes propagate, i.e., between the boundaries of a one-dimensional cantilever plate into an infinite domain. This concept is shown in Figure 3, where the bold line represents the waves propagating in the structure and the dashed line represents the waves in the infinite domain by the method of image. As the waves will encounter a 180° phase shift, the wave modes will be discontinuous when a fixed-end is encountered. This discontinuity in turn limits the adoption of a two-sided Laplace transform as shown in Equation (11) into the sensor equation (10). The spatial weighting characteristic of the distributed sensor offers a design freedom to overcome the nature of this discontinuity by setting the weighting factor to zero at the locations where the discontinuous waves occur.

In an earlier paper by the authors (Hsu and Lee, 2002), they proposed that zero weighting at the boundaries was to be realized by subtracting a sine or a cosine function of a suitable scaling factor to the chosen base, which was developed based on the fact that a two-sided Laplace transform of a sine or a cosine function is zero. It should be noted that the predetermined base was not modified, i.e., the induced filtering effect was a result of the predetermined base only.

In this article, in comparison, we incorporate the mathematical tool window functions (Harris, 1978) to overcome the nature of this discontinuity. The application herein is similar to those used to design surface acoustic wave devices (SAW devices) (Campbell, 1989, 1998). Another similarity worth noting is that the SAW devices can exert the same autonomous phase–gain relationship as the APROPOS device discussed in this study. To handle the case where the wave modes are discontinuous at the boundary points, the window functions are multiplied to the chosen base so that the product becomes zero at the boundaries (Figure 3). Thus, this new design is a completely different mathematical manipulation that causes significantly different filtering effects from the earlier reports. In addition to possessing the ability to completely eliminate the effect of the boundaries, additional spatial design parameters can be introduced through the window functions. More specifically, this newly designed APROPOS device possesses the ability to tailor the filtering effect of the chosen base by changing the parameters of the window functions.

By utilizing the above-mentioned concept provides us with a path to transfer the wave modes of finite sensor structures to wave modes located in the infinite domain. Thus, Equation (10) can now be rewritten as (Hsu and Lee, 2002):

$$q(t) = -z_k^o e_{31} e^{j\omega t} k^2 \left[ -w_{lp} \int_{-\infty}^{\infty} f(x) e^{jkx} dx - w_{rp} \right.$$
$$\times \int_{-\infty}^{\infty} f(x) e^{-jkx} dx + w_{le} \int_{-\infty}^{\infty} f(x) e^{kx} dx$$
$$\left. + w_{re} \int_{-\infty}^{\infty} f(x) e^{-kx} dx \right] \tag{12}$$

where

$$f(x) = h(x)R(x) \tag{13}$$

$h(x)$ is the window function multiplied to tailor the surface electrode $R(x)$, and where the real effective surface electrode to be implemented becomes $f(x) = h(x)R(x)$ (Figure 4). This perspective provides us with an opportunity to further tailor the performance of distributed sensors when applied on a small testing structure and to design the so-called PoD sensors. Once the wave modes are expanded onto the infinite domain by using the above-mentioned concept, the propagating waves and the evanescent waves can all be taken into account when designing autonomous gain–phase
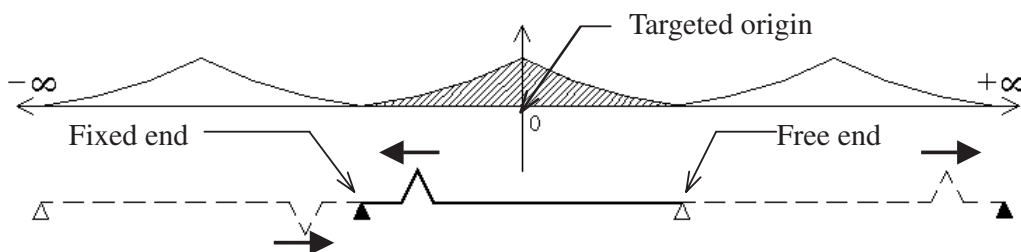


**Figure 3.** Wave mode expansions on a cantilever plate by implementing method of image and an APROPOS device designed by window functions.
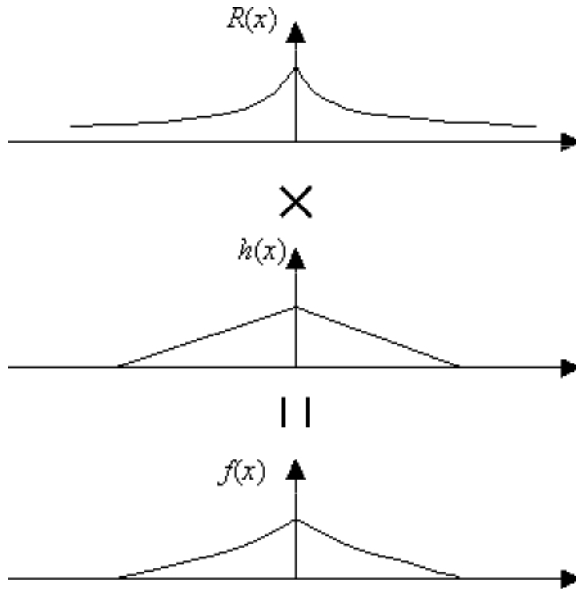
**Figure 4.** *Schematic of an APROPOS device designed by window functions.*

sensors. In addition, the contributions of the boundaries can also be eliminated. Thus, continuous wave modes are reconstructed in an infinite domain by the APROPOS device and the sensor equation can thus be rewritten as a two-sided Laplace transform, which enables the introduction of a no-phase delay filter in the spatial domain.

Another concept worth noting is related to the symmetry of the wave modes. It is well known that in all wave equations, waves always appear in pairs, i.e., the left and the right propagating waves as well as evanescent waves exist simultaneously with respect to the origin (Figure 3). Based on this concept, choosing an effective surface electrode with a symmetric profile with respect to origin $x = 0$, Equation (12) can be rewritten as (Hsu and Lee, 2002):

$$q(t) = -z_k^0 e_{31} e^{j\omega t} k^2 \left[ -(w_{lp} + w_{rp}) \int_{-\infty}^{\infty} f(x) e^{-jkx} dx \right.$$
$$\left. + (w_{le} + w_{re}) \int_{-\infty}^{\infty} f(x) e^{-kx} dx \right] \quad (14)$$

where the origin can be placed at any location of the structure and the combination of the effective surface electrode $f(x)$ and wave modes is symmetric with respect to this origin, which we call a targeted origin (Figure 3). It should also be noted that the configuration of the wave mode amplitudes depends on the targeted origin chosen. Even though a more detailed design thinking relating to the targeted origin placement was the main subject of a separate paper (Hsu and Lee, 2002), it is clear from Equation (14) that the filtering effect introduced by the APROPOS device comes from the integration of the effective surface electrode and the wave modes. Another thing that should be noted is that

the wave mode amplitudes are outside of the integration, since they are a function of the wave number $k$ only. That is, the filters being introduced into the sensor charge output and the sensor transfer function have their strain information originating from the wave mode of the infinite domain. The wave mode amplitude represents the local structure characteristics of a symmetric point on the effective surface electrode chosen, i.e., the targeted origin. This point can easily be understood by substituting $x = 0$ to the second derivative of the bending angle with respect to the spatial coordinate $x$ as shown in Equation (9), i.e.,

$$w''(x = 0, t) = k^2[-(w_{lp} + w_{le}) + (w_{rp} + w_{re})]e^{j\omega t}. \quad (9a)$$

More specifically, the filter introduced is actually designated with respect to the symmetric point of the effective electrode and this point is thus named the targeted origin in designing APROPOS devices (Figure 3).

In the above-mentioned configuration, the APROPOS device serves as a point sensor of the attached testing structure, like the cantilever plate shown in Figure 1. In other words, the APROPOS device is a point sensor measuring the local structure characteristic of the targeted origin, and its transfer function is further tailored by the symmetrically distributed effective surface electrode in the spatial domain. As the PoD sensor was implemented using the APROPOS device concept, the sensor performance is thus the result of the superposition of the full characteristics of the sensor structure itself, the local characteristics of the targeted origin, and the no-phase-delay low-pass filter created by the surface electrode.

The above-mentioned symmetric observations can be used to explain the reason why the APROPOS devices can be introduced to a low-pass filter without any phase lag and which is different from the Bode gain–phase theorem (Bode, 1945) prediction, from an almost philosophical perspective. As the original Bode gain–phase theorem states that the gain and phase of a causal system is not autonomous, the assertion that APROPOS devices can break free of this theorem indicates that the system appears to act like a noncausal system. Taking all the parameters into consideration such as the symmetry of the wave modes mentioned above, the dispersion relationship (Equation (8)) of the sensor structure, and the general solution of the wave equation (Equation (9)), it appears that the left and the right wave modes act like the past and the future time information at any point of the sensor structure. That is, the signal of the future and the past exists at the same time for any point of the sensor structure. The sensor structure designed based on the above-mentioned concept thus acts like a noncausal system and can perform gain tailoring without sacrificing phase performance.

The possibility to enhance the sensor performance was conceptually proven by properly choosing the

targeted origin and the effective surface electrode using the APROPOS device concept as shown in Equation (14). We can conclude that an APROPOS device is a distributed sensor that can measure the local structure information of a specific point on a flexible structure, and which possesses no-phase delay filtering effects through spatial domain integration. In addition, it offers a full solution to incorporate the advantages of distributed sensors into point sensor design, i.e. PoD sensors, where both the low-frequency sensitivity and the usable bandwidth are appropriately accounted for. In the following section, an APROPOS device based on the methodologies of window functions and the method of image will be detailed.

## IMPLEMENTING APROPOS DEVICES WITH WINDOW FUNCTIONS

As mentioned earlier, choosing a proper window function, $h(x)$ and multiplying it to the effective surface electrode, $R(x)$ in order to create a no-phase lag low-pass filter into the sensor structure frequency response with tunable parameters is a main goal of this article. That is, the autonomous gain–phase sensors which have poles of various orders are of special interest to us due to the implication that they can work as a series of low-pass filters. The fundamental performance characteristics of these sensors can be understood by examining the functions shown in Table 1 (Grossman, 1988, O'Neil, 1991). For example, considering a window function of the following form

$$w(x) = 1 - |x|^n/a^n, \qquad (15)$$

where $|x| \leq a$, and $a$ is the half length of the beam. With this window function and choosing the base to have a form of $e^{-\alpha|x|}$, the effect of the PoD sensor can be studied by performing the following Laplace transform as shown in Equation (11) (Van Der Pol and Bremmer, 1959; O'Neil, 1991). It should be noted that the base of this APROPOS device was intentionally chosen to be identical to the authors' earlier report (Hsu and Lee, 2002) so as to clearly show the differences of the characteristics obtained by using these two lines of methods adopted. The results are

$$\int_{-a}^{a} \left[ \left( 1 - \left( \frac{|x|}{a} \right)^n \right) e^{-\alpha|x|} \right] e^{-sx} dx$$

$$= \frac{[a^n(s+\alpha)^n] - n!}{a^n(s+\alpha)^{n+1}} + \frac{[a^n(\alpha-s)^n] - n!}{a^n(\alpha-s)^{n+1}}$$

$$= \frac{2\alpha(\alpha^2-s^2)^n - (n!/a^n)[(\alpha-s)^{n+1} + (\alpha+s)^{n+1}]}{(\alpha^2-s^2)^{n+1}}. \quad (16)$$

where the transform parameter $s$ is $jk$ for the first integral in Equation (14) or $k$ for the second integral in

### Table 1. (a) Right-sided Laplace transformed pair where $F(s) = \int_0^a f(x)e^{-sx} dx$; (b) left-sided Laplace transforme pair where $F(s) = \int_{-a}^0 f(x)e^{-sx} dx$.

| $f(x)$ | $F(s) = L\{f(x)\}$ |
| --- | --- |
| a | |
| $e^{-at}$ | $\dfrac{1}{s+a}$ |
| $t^n e^{-at}$ | $\dfrac{n!}{(s+a)^{n+1}}$ |
| b | |
| $e^{at}$ | $\dfrac{1}{a-s}$ |
| $-|t|^n e^{at}$ | $-\dfrac{n!}{(a-s)^{n+1}}$ |

Equation (14). Considering Equation (16), it should be noted that the poles of the system are a power of $n+1$ function of $(\alpha^2 - s^2)$. We can see that $1/(\alpha^2 - s^2)$ was caused by the two-sided Laplace transform of base $e^{-\alpha|x|}$ and is the same as the results reported earlier (Hsu and Lee, 2002). It can also be seen that Equation (16) has three additional parameters introduced by the window functions that are embedded into the induced filter. These parameters include the power of the window functions adopted, the desired corner frequency, and the length of the sensor structure. In other words, the APROPOS device acts like a no-phase delay low-pass filter with three tunable variables. We can also see that all the odd power functions of $s$ in the numerator are cancelled automatically for all $n$. Therefore, no matter whether $n$ is odd or even, the numerator will be an even power term of $s$. It is known that this type of function can only be expanded into a product of the term involving only $(\beta^2 - s^2)^n$, $(s^2 + as + b^2)$, and $(s^2 - as + b^2)$, where $\beta$, $a$, and $b$ are constants. More specifically, the filtering effect induced in the sensor signal from Equation (16), which is an integral effect of the propagating wave and the evanescent wave, has the following form such that

$$F(s) = c \frac{\prod_{i=1}^{\bar{n}} \left( \beta_i^2 - s^2 \right)^{\bar{l}_i} (s^2 - a_i s + b_i^2)^{\overline{m}_i} (s^2 + a_i s + b_i^2)^{\overline{m}_i}}{(\alpha^2 - s^2)^{n+1}}$$

(17a)

where

$$n = \sum_i^{\bar{n}} \left( \bar{l}_i + 2\overline{m}_i \right) \qquad (17b)$$

$\beta_i$, $a_i$, $b_i$, $\overline{m}_i$, $\bar{l}_i$, and $\bar{n}$ are constants determined by Equation (16), $\alpha$ is the prespecified corner wave number, and $c$ is a function of $\alpha$, i.e., $c = c(\alpha)$. Note that the zeros formed by the $(s^2 + as + b^2)$, and the $(s^2 - as + b^2)$ pairs introduced by using the APROPOS device will not cause any delay into the sensor special transfer function.

Substituting the dispersion relationship of propagating waves in Equation (8b) for the case where the transform parameter $s$ is $jk$ in Equation (17a), Equation (17a) can be transferred from a wave number domain to a frequency domain such that

$$F(\omega) = c \frac{\prod_{i=1}^{\bar{n}} (\bar{\beta}_i + \omega)^{\bar{l}_i} \left[ (\omega + \bar{b}_i)^2 + \bar{a}_i \omega \right]^{\bar{m}_i}}{(\bar{\alpha} + \omega)^{n+1}} \quad (18)$$

where $\bar{\beta}_i$, $\bar{b}_i$, $\bar{a}_i$ are transferred constants derived from $\beta_i$, $a_i$, $b_i$, and $\bar{\alpha}$; is the chosen corner frequency from $\alpha$ by using the dispersion relationship. Similarly, substituting the dispersion relationship of the evanescent waves in Equation (8c) for the case where the transform parameter $s$ is $k$ in Equation (17a), Equation (17a) is again transformed to Equation (18). By varying the three embedded design parameters in the transferred constants $\bar{\beta}_i$, $\bar{b}_i$, $\bar{a}_i$ leads to an APROPOS device that possesses tunable filtering characteristics in a frequency domain. It is clear from Equation (18) that both the poles and zeros have a no-phase change in a frequency domain. Thus, the signal of the designed APROPOS device can be expressed as follows:

$$q(t) = -z_k^0 e_{31} e^{j\omega t} k^2 \left[ -(w_{lp} + w_{rp}) + (w_{le} + w_{re}) \right] F(\omega) \quad (19)$$

Equation (19) shows that the APROPOS device exerts its influence by multiplying a pure real-value roll-off function to the four wave mode amplitudes, which represent the characteristics of the structure and targeted origin. Note that the induced filter shown above is a $-40$ dB/decade low-pass filter in a wave number domain (Equation (17a)), and is a $-20$ dB/decade low-pass filter in the frequency domain (Equation (18)). Incorporating an APROPOS device to a PoD sensor will result in an autonomous gain–phase filter (Equation 19) to be multiplied to each wave mode of the sensor structure. With the adoption of a window functions concept, three powerful design parameters that include the length of the sensing structure $2a$,

the corner frequency $\alpha$ and the power of the window function $n$, allow us to tailor the desired performance of the PoD sensor of interest. Thus, a different mathematical action to the design of the weighting function offered by the effective surface electrode can have a completely different filtering effect in a wave number domain. In Table 2, we summarize and compare the characteristics of the APROPOS device implemented by the subtraction of a sine or a cosine function and by multiplying a window function to the designed base.

Since the sensor response of the APROPOS device is really a combination of a sensor structure response and an effective surface electrode sensor, the added benefit of introducing a distributed sensors concept into point sensors to create PoD sensors must be examined by removing both the effect of the sensor structure response and the targeted origin response. This removal was done by simultaneously measuring the strain located at the targeted origin of the beam and the newly developed APROPOS device, which measure the local strain (Equation (9a)) at $x = 0$ and such that Equation (19) can be further written as:

$$q(t) = -z_k^0 e_{31} F(\omega) [(w''(x = 0, t))] \quad (19a)$$

More specifically, dividing the distributed piezoelectric sensor response with respect to the strain of the targeted origin clearly demonstrates the added benefit of the APROPOS devices in Equation (18), which is the filtering effect expressed by $F(\omega)$. It can be experimentally shown that the PoD sensors can be designed to have the gain transfer functions tailored into the sensor while keeping the phase transfer functions intact.

## EXPERIMENTAL SETUP

To experimentally verify the concepts of how an APROPOS device can be adopted to improve the performance of a PoD sensor, a 140 mm long × 22 mm

**Table 2. Comparison of APROPOS devices designed by subtracting a sine or a cosine function (A) and by multiplying a window function (B).**

|  | (A) | (B) |
|---|---|---|
| Methodology | (1) Method of image<br>(2) Superposition of integration | (1) Method of image<br>(2) Window function |
| Mathematical action | Subtraction | Multiplication |
| Applied function | Sine/cosine function | Window function |
| Advantages | (1) Simple and direct<br>(2) No need to consider how the sensor transfer function will be altered<br>(3) Contribution of the APROPOS device is completely determined by the base | (1) Simple and direct<br>(2) No need to fine tune a subtracted function to make zero weighting at the boundaries<br>(3) Additional design parameters can be introduced through the window functions |
| Characteristics of filters | Predetermined no-phase-delay filters can be designed by choosing a proper base | (1) Tunable no-phase-delay filters can be embedded by the window function<br>(2) Various filtering effect can be implemented by tailoring the embedded parameters |

(a)



(b)
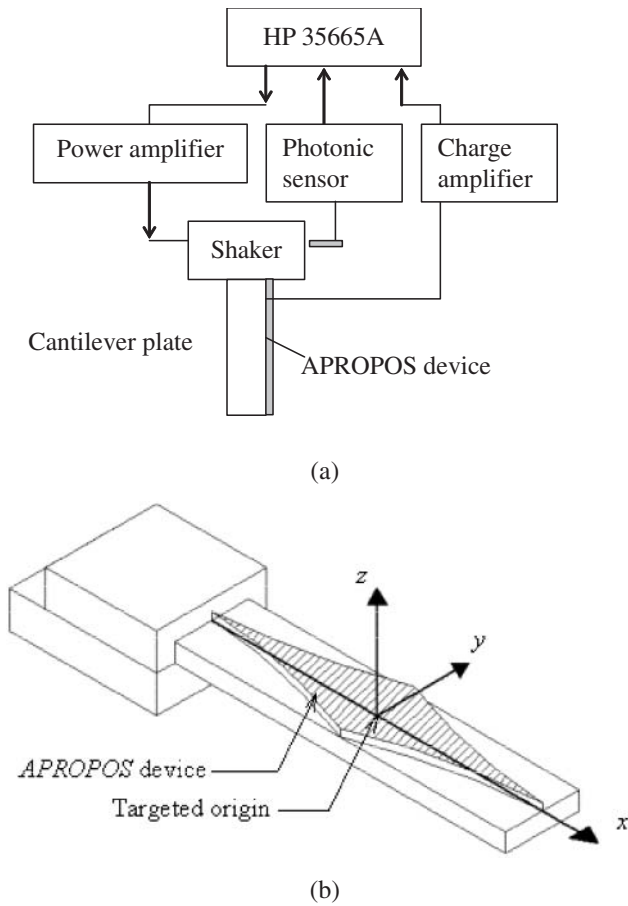
**Figure 5.** *(a) Schematic of the experimental setup and (b) schematic of an APROPOS device designed by window functions.*



**Figure 6.** *Transfer functions of a point sensor with a uniform surface electrode (thick gray line) and an APROPOS device with no-phase-delay low-pass filter (thin dark line).*

wide × 0.02 mm thick stainless steel shim in one-dimensional cantilever plate configuration was chosen as the base sensor structure. To further examine the effect of APROPOS devices, a piezoelectric distributed sensor that had a uniform effective surface electrode and window function of $n = 1$ was also constructed. The setup of the experiment executed and the shape of the effective surface electrode are shown in Figure 5(a) and (b). The targeted origin of the APROPOS device was placed at the middle of the cantilever plate. Although, the cantilever plate was small, the effect of the boundaries and the evanescent waves cannot be neglected. Two perspectives can be used to examine this cantilever plate configuration. First, when this one-dimensional cantilever sensor plate structure is observed from the classical flexible structure concept, the stainless steel shim can be considered as the flexible structure to be controlled. Second, this cantilever plate can be viewed as a point sensor with its performance tailored by using an APROPOS device. In addition, it should be noted that the ratio between the sensor size and the sensor structure dictates that the boundary effects and the evanescent wave modes cannot be neglected as was done earlier when the spatial filter was first introduced (Miller et al., 1990).
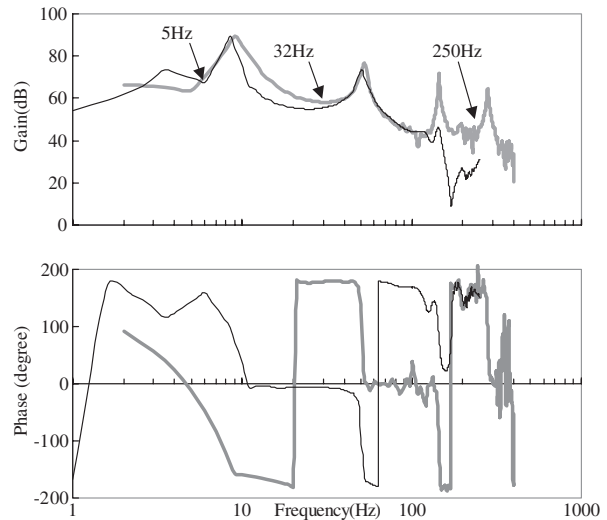
Three main design parameters were chosen to implement the desired gain tailoring characteristics. They include the power $n$ of the window function (see Equation (16)), the length of the sensor structure $2a$, and the desired location of the corner frequency of the low-pass filter. Using the natural frequency measured from the uniform sensor in Figure 6 (thick gray line), with 9 and 56 Hz as the first and the second mode natural frequencies, respectively, the parameters needed to calculate the dispersion relationship in Equation (8) were retrieved by using the experimental results. Using Equation (4) to calculate the physical quantity measured by using the uniform sensor led to the angular deflection of the free-end. On the other hand, the signal retrieved by the APROPOS device is a filtered strain signal of the targeted origin (Equation (19)). The transfer function of the uniform sensor must then incorporate a $jk$ term to form a compatible result in the wave-number domain. By using the dispersion relationship of the one-dimensional plate shown in Equation (8), the transfer function in a frequency domain requires adding $10 \times \log_{10}(\omega)$ to the measured data of the uniform sensor. Substituting the numerical normalized wave number $\lambda_i$ (Blevins, 1979), set $k$ equal to $\lambda_i/L$, with $L$ as the length of the structure with $k$ equal to 1.8751 and 4.694 for the first and the second natural modes, respectively. Substituting the data into Equation (8), we can derive that the material property $D_{11}/\rho A$ is 0.101846. Choosing a corner wave number $k = 10$ in the spatial domain and substituting all the corresponding parameters into the dispersion relationship, Equation (8) leads to a corner frequency, $\alpha = 32$ Hz. The effective surface electrode was chosen to be:

$$w(x) = 1 - \frac{|x|}{a}, \qquad (20)$$

where $a$ is 0.07 m. From Equations (18) and (19), it is clear that the no-phase-delay low-pass filter, i.e., an autonomous phase–gain filter, introduced by this APROPOS device with $n = 1$ from Equation (17) is

$$f(\omega) = -48.571 \frac{(5 - \omega)}{(32 + \omega)^2} \qquad (21)$$

Combining Equations (8) and (21), it is clear that a zero is introduced at 5 Hz. This zero will introduce a $-180°$ phase lag at the frequency range lower than 5 Hz, and a no-phase lag for frequencies higher than 5 Hz. The appearance of the extra zero that introduces the phase lag can be attributed to the case where the design parameter $n$ was set to be equal to 1 and the $(s^2 + as + b^2)$ and the $(s^2 - as + b^2)$ pairs do not appear in the numerator; otherwise it would cancel their respective phase distributions, It should be noted that the influence of this zero is completely eliminated by either choosing different design parameters or by introducing another window function. Equation (21) also showed that an APROPOS device designed by multiplying a window function to a chosen base can tailor the filter effect of the base, i.e., converting the original first-order pole $1/(32 + \omega)$ to a second-order pole $1/(32 + \omega)^2$ and to a zero $(5 - \omega)$. This zero can be used to change the sign of the output signal or to reject some particular frequency range signals. Note also that the original no-phase-delay low-pass filter designed by the base is retained and enhanced, which is contributed by multiplying a window function. Thus using a window function to modify a base can introduce additional tunable parameters into the induced filters, which in turn allows the implemented APROPOS device to possess new filtering characteristics.

Substituting the boundary conditions of a one-dimensional cantilever plate with excitation from a fixed-end into Equation (9), it is easy to derive the four wave mode amplitudes at the targeted origin, which is set at the middle of the cantilever plate:

$$w_{lp} = \left[ \frac{\left[(j + 1)e^{4ak} + j - 1\right]e^{jak} + 2je^{3jak + 2ak}}{8je^{2jak + 2ak} + (2je^{4ak} + 2j)e^{4jak} + 2je^{4ak} + 2j} \right] g$$
$$(22a)$$

$$w_{le} = \left[ \frac{(j - 1)e^{4jak + ak} + 2je^{2jak + 3ak} + (j + 1)e^{ak}}{8je^{2jak + 2ak} + (2je^{4ak} + 2j)e^{4jak} + 2je^{4ak} + 2j} \right] g$$
$$(22b)$$

$$w_{rp} = \left[ \frac{\left[(j - 1)e^{4ak} + j + 1\right]e^{3jak} + 2je^{jak + 2ak}}{8je^{2jak + 2ak} + (2je^{4ak} + 2j)e^{4jak} + 2je^{4ak} + 2j} \right] g$$
$$(22c)$$

$$w_{re} = \left[ \frac{(j + 1)e^{4jak + 3ak} + 2je^{2jak + ak} + (j - 1)e^{3ak}}{8je^{2jak + 2ak} + (2je^{4ak} + 2j)e^{4jak} + 2je^{4ak} + 2j} \right] g$$
$$(22d)$$

It should be noted that the denominators of the four wave modes are identical and the numerators of these wave modes dictate the effects of the propagating and the evanescent wave modes. Summing the corresponding numerators and considering that $|e^{jak}| = 1$ and $e^{ak}$ dominates for the high wave numbers, the magnitude of the propagating wave modes and the evanescent wave modes becomes

$$w_{lp} + w_{rp} \approx e^{jak}(e^{2ak} + 1)\left[2(e^{2ak} + 1) + j(e^{2ak} - 1)\right] \quad (23a)$$
$$w_{le} + w_{re} \approx e^{ak}(e^{2jak} + 1)\left[2(e^{2ak} + 1) + jA\right] \qquad (23b)$$

where $A$ approaches zero. Further simplifying Equations (23a) and (23b) yields the wave mode amplitude of the propagating and the evanescent waves of the cantilever plate at a high frequency or wave number such that

$$|w_{lp} + w_{rp}| \approx \sqrt{5}e^{4ak}, \qquad (24a)$$

and

$$|w_{le} + w_{re}| \approx 2e^{3ak}. \qquad (24b)$$

Substituting first the effect that $D_{11}/\rho A = 0.101846$ into Equation (8) and then into Equations (24a) and (24b) leads to the understanding that the magnitude of the evanescent wave is more than 10% of the magnitude of the propagating wave when the frequency is less than 256 Hz, or when the wave number is less than 28.322. In other words, the effect of the evanescent wave cannot be neglected when the frequency of interest is less than 256 Hz. Since the designed corner frequency is chosen to be at 32 Hz, then the APROPOS device will certainly encounter the contribution of the evanescent waves.

The transfer function shown by the thick gray line in Figure 6 of the point sensor can be tailored by using Equation (20) as the effective surface electrode. The experimental data of the tailored transfer function is shown by the thin dark line in Figure 6. Comparing the two experimental data as shown in Figure 6, it is clear from the experimental data obtained that a no-phase delay low-pass filter is indeed introduced by using an APROPOS device and that the theoretical predictions agree well with the experimental results. The additional zero that are introduced offers a $-180°$ phase lag below 5 Hz, and offers no additional phase contribution after several hertzs at its corner frequency. In addition, the no-phase low-pass filter induced by the low-pass filter $1/(32 + \omega)^2$ in Equation (21) introduces no additional phase information into the transfer function throughout the full frequency range, including at its corner frequency of 32 Hz.

To further illustrate the effect of the newly introduced no-phase-delay low-pass filter, the ratio between the signals obtained by using Equation (20) as the effective surface electrode, i.e., the filtering effect introduced by using Equation (21) and from a strain gage located at the
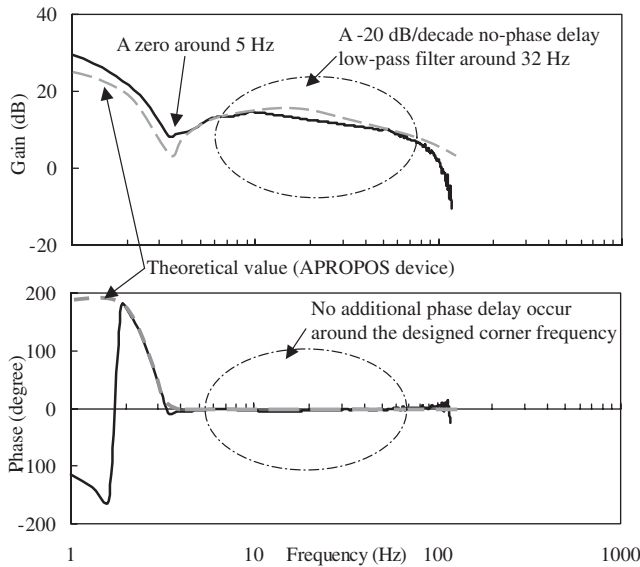
**Figure 7.** A no-phase-delay low-pass gain tailoring effect of the transfer function of a PoD sensor (dark line) and its theoretical value (gray dashed line).

targeted origin of the PoD sensor, is shown in Figure 7. The dark solid line in Figure 7 represents the experimental data and the gray broken line represents the theoretical predictions. The agreement between the experimental data and the theoretical predictions clearly demonstrates the validity and the effectiveness of the APROPOS device as presented in this article. It should also be clear that the effectiveness of the above-mentioned approach is traceable to the fact that the APROPOS devices are introduced outside of the wave mode amplitudes. This indicates that APROPOS devices can actually perform filtering effects in an infinite domain. In summary, the information induced by the wave mode amplitudes, which are the same character-istics as the structure and the local performance at the targeted origin, can be retrieved by dividing the signal from a strain gage placed at the targeted origin. The zero of around 5 Hz was induced by the APROPOS device, which can be eliminated by choosing the appropriate design parameters including the power of window functions, the corner frequency, and the length of the sensor structure.

## CONCLUSIONS

Both the theoretical and the experimental results verified the successful implementation of autonomous gain–phase sensors, i.e., the APROPOS device-based sensors. In addition, the possibility of improving the performance of a Point-distributed sensor (PoD) by taking advantages of the characteristics of autonomous gain–phase tailoring was shown. The design parameters of a series of low-pass filters using an APROPOS device were detailed. The proper range for the design param-

eters was also verified theoretically and experimentally. We also introduced window functions in the sensor design process, which equals zero near and at the boundaries. With the introduction of the window functions, the targeted origin of the distributed sensor can be placed near the boundaries. In addition, the APROPOS device can be used to design point sensors even for cases where the testing structure is too short to neglect the boundary and evanescent waves effects.

Even though an APROPOS device-based PoD sensor represents a very special type of filter, such that it can have gain tailoring while remaining at a zero phase change, many of the filter design concepts developed over the years for the traditional electronic-based filters can still be modified to adopt a PoD sensor design. By properly choosing the power of the window functions, the corner frequency, the length of the sensor structure, etc., PoD sensors of various performance specifications were shown to be possible. One thing that should be noted is that even though in this paper, we only discussed a PoD sensor that uses a one-dimensional cantilever plate as the base structure, PoD sensors based on other base structures can certainly be used. It should be clear from the results presented in this article that different boundary conditions simply lead to different $w_{rp}$, $w_{lp}$, $w_{re}$, $w_{le}$, which in turn influence the overall sensor transfer functions. Nevertheless, the design concept described in this article is applicable to all types of boundaries.

In summary, PoD sensors developed by adopting an APROPOS device were invented. With full integration of a distributed sensor concept and the more traditional point sensor, the results presented in this article are far reaching and have a fundamental impact on the design of all point sensors.

## REFERENCES

ANSI/IEEE Standard 176, (Sept. 1987). *Piezoelectricity*, Institute of Electrical and Electronics Engineers, Inc. (http://standards.ieee.org/catalog/oils/arch ultrasonics.html)

Blevins, R.D. 1979. *Formulas for Natural Frequency and Mode Shape*, pp. 108–109, Robert E. Krieger Publishing Co. Inc., Florida, USA.

Bode, H.W. 1945. *Network Analysis and Feedback Amplifier Design*, D. Van Nostrand, New York, New York, USA.

Bracewell, R.N. 1978. *The Fourier Transform and Its Application*, 2nd edn, McGraw-Hill, New York, USA.

Cady, W.G. 1946. *Piezoelectricity*, Vol. 1, pp. 1–8, McGraw-Hill, New York, New York, USA.

Campbell, C.K. 1989. *Surface Acoustic Wave Devices and their Signal Processing Applications*, Academic Press Inc., Boston, Massachusetts, USA.

Campbell, C.K. 1998. *Surface Acoustic Wave Device for Mobile and Wireless Communications*, Academic Press Inc., San Diego, CA, USA.

Fung, Y.C. 1965. *Foundation of Solid Mechanics*, Prentice-Hall Inc., Englewood Cliffs, New Jersey, USA.

Graff, K.F. 1975 *Wave Motion in Elastic Solids*, Dover Publications Inc., New York, New York, USA.

Grossman, D. 1988. *Advanced Engineering Mathematics*, Harper and Row, New York, New York, USA.

Harris, F.J. 1978. "On the Use of Windows for Harmonic Analysis with Discrete Fourier Transform," *Proceedings of the IEEE*, 66(1):51–83.

Hsu, Y.H. and Lee, C.K. June 2002 "Targeted Origin Placement for the Autonomous Gain-Phase Tailoring of Piezoelectric Sensors," *Smart Materials and Structures*, 11(3):444–458.

Hsu, Y.H. and Lee, C.K. March 2003 "Autonomous Gain-Phase Tailoring of Rotational Acceleration Rate Sensors," *AIAA Journal*, 41(3):549–551.

Kawai, H. 1969. "The Piezoelectricity of Poly(vinylidene fluoride)," *Japan Journal of Applied Physics*, 8:975–976.

Lee, C.K. March, 1990. "Theory of Laminated Piezoelectric Plates for the Design of Distributed Sensors/Actuators: Governing Equations and Reciprocal Relationships," *J. Acoust. Soc. Am.*, 87:1144–1158.

Lee, C.K. December 1992. "Piezoelectric Laminates: Theory and Experiments for Distributed Sensors and Actuators," In: Tzou, H.S. and Anderson, G.L. (eds.), *Intelligent Structural Systems*, pp. 75–167, Kluwer Academic Publishers, Netherlands Dordrecht.

Lee, C.K. and Moon, F.C. June 1990. "Modal Sensors/Actuators," *ASME Journal of Applied Mechanics*, 57:434–441.

Miller, D.W., Collins, S.A. and Peltzman, S.P. 1990. "Development of Spatially Convolving Sensors for Structural Control Applications," In: *Proceedings of the AIAA/ASME/ASCE/AHS Structures, Structural Dynamics, and Materials Conference*, Long Beach, CA, USA, pp. 2283–2297.

O'Neil, P.V. 1991. *Advanced Engineering Mathematics*, 3rd edn, PWS, Boston, Massachusetts, USA.

Prak, A., Elwenspoek, M. and Fluitman, J.H.J. December 1992. "Selective Mode Excitation and Detection of Micromachined Resonators," *Journal of Microelectromechanical Systems*, 1(4):179–186.

Preumont, A. and Francois, A. 1999. "Piezoelectric Array Sensing for Real-Time, Broad-Band Sound Radiation Measurement," In: *Proc. of International Conference on Adaptive Structure and Technologies* (*ICAST'99*), October 11–13, Paris, France, pp. 37–44, Technomic Publishing Co. Inc., Lancaster, Pennsylvania, USA.

Tzou, H., Zhong, S.J.P. and Natori, M. January 1993. "Sensor Mechanics of Distributed Shell Convolving Sensors Applied to Flexible Rings," *Transactions of the ASME*, 115:40–46.

Tzou, H.S. and Hollkamp, J.J. May 1994. "Collocated Independent Modal Control with Self-Sensing Orthogonal Piezoelectric Actuators (Theory and Experiment)," *Smart Materials and Structures*, 3:277–284.

Van Der Pol, B., and Bremmer, H. 1959. *Operational Calculus*: *Based on the Two-Sided Laplace Integral*, Am. Mathematical Society, 2nd edn, Paris, in French.